

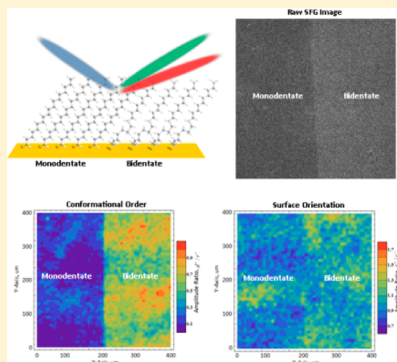
Image Contrast in Sum Frequency Generation Microscopy Based on Monolayer Order and Coverage

Joon Hee Jang, Jack Jacob, Gregg Santos, T. Randall Lee, and Steven Baldelli*

Department of Chemistry, University of Houston, Houston, Texas 77204-5003, United States

Supporting Information

ABSTRACT: Sum frequency generation imaging microscopy (SFGIM) was used to study a binary system of self-assembled monolayers (SAMs) on evaporated gold. A two-step process that consists of microcontact printing (μ CP) and the solution backfilling method is used to generate a sample surface with two distinct SAMs domains. The high contrast chemical identification and the homogeneity map of the SAMs for two different head groups are revealed by processing the three-dimensional images (xy -surface and infrared wavenumbers) obtained from SFGIM. For conformation order analysis, the amplitude ratios of the methylene and methyl symmetric resonance obtained by a nonlinear curve fit of the spatially and spectrally resolved SFG images are used to reconstruct spatial image maps. The conformation order map shows the distribution of gauche defects in SAMs with improved contrast across monodentate and bidentate alkanethiol monolayer regions. The results show that variation of the head group attached on the surface dominantly influences the conformation disorder and surface coverage of the molecules, while the terminal methyl group in both monodentate and bidentate SAMs shows a similar orientation angle.



1. INTRODUCTION

Self-assembled monolayers (SAMs) are assemblies of surfactant molecules on the surface formed by spontaneous chemical absorption. Molecules in a SAM consist of a head group, which has a strong affinity for the substrates, and a tail group that can be modified to alter the chemical characteristics of the surface. The strong chemisorption of a head group to the surface atoms and the van der Waals interactions between the hydrophobic chains provide stable and well-packed monolayers. The functionality of a tail group offers surface property modification for various applications of SAMs such as corrosion inhibition, wetting, lithography, and crystallization.^{1–3}

The most studied SAMs systems are the long-chain alkanethiols on the gold surfaces. Several studies on the thermodynamic energy including the formation of SAMs on the gold surface show that the chemisorption enthalpy of the sulfur–gold bond is about 130 kJ/mol with an activation energy of 30 kJ/mol.^{4,5} The two-step assembly process is the most accepted mechanism of SAM formation, as suggested by contact angle and ellipsometry measurements.^{6,7} A rapid adsorption of the alkanethiols on the gold surface within the first few minutes is followed by a slow step lasting several hours until the formation of the monolayer is completed. The packing density of a well-ordered monolayer is reported to be $\sim 4 \times 10^{14}$ chains/cm².⁸

A number of studies on the surface properties of the SAMs on metal utilizing various surface characterization methods have been published. The chemical composition and structure at the surfaces are studied by spectroscopic techniques such as photoelectron spectroscopy, vibrational spectroscopy, and

nonlinear spectroscopy.^{9–15} Microscopic techniques, such as atomic force microscopy and scanning tunneling microscopy, reveal the surface morphology with atomic spatial resolution.^{9,12,16} These studies show that the surface properties greatly depend on the conformation, orientation, monolayer density, and homogeneity of SAMs.

Surface patterning techniques that form SAMs with spatial resolution have been developed and provide a useful process for lithography, molecular electronics, and biological applications.^{3,17,18} Microcontact printing (μ CP) is the most widely used method to produce a patterned surface of mixed SAMs with submicrometer spatial resolution.¹⁷

While most conventional surface probing techniques provide either morphology or chemical identification, a recently developed sum frequency generation imaging microscopy (SFGIM) technique has been proven to be effective in analyzing the SAMs patterned surfaces, revealing both spatial and chemical resolution without the need for labeling the chromophore or fluorescent probe.^{19,20} Spatially resolved images from SFGIM can be used to generate a chemical map of the surface-specific interests such as orientation, distribution, and conformation order of absorbed molecules localized on the surface. Cimatu et al. analyzed spatially controlled surface monolayers with various terminal groups using SFGIM.²¹ In the study, μ CP stamped and backfilled SAMs on the gold substrate with different terminal groups were analyzed with

Received: May 11, 2013

Revised: June 26, 2013

Published: July 11, 2013



SFGIM. Images were produced based on the chemical contrast of the SAMs with a spatial resolution of $\sim 2 \mu\text{m}$. In addition to the terminal group, the homogeneity of SAMs with various head groups has been examined in terms of the orientation and conformation distribution.²² However, spatially resolved chemical contrast of SAMs with the same tail but different head groups bound on the same surface has not been studied.

In this work, a binary system of monodentate and bidentate long-chain alkyl thiols on gold has been analyzed using SFGIM. The molecular structure of monodentate and bidentate is illustrated in Figure 1. By reconstructing the intensity ratio map and histogram, the chemical contrast of SAMs with two different head groups is presented.

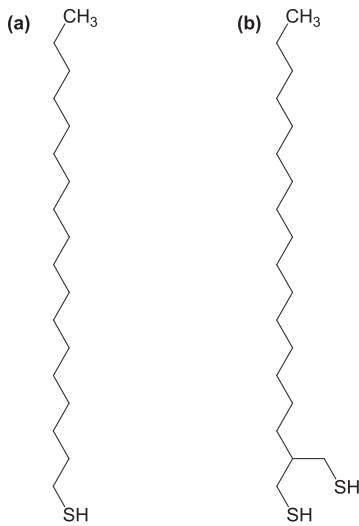


Figure 1. Molecular structure of (a) octadecanethiol (monodentate) and (b) 2-hexadecylpropane-1,3-dithiol (bidentate).

2. BACKGROUND

SFG is a coherent three-photon second-order nonlinear spectroscopic technique that is sensitive to the orientation of surface molecules. A mid-infrared (IR) and a visible beam are overlapped on a surface at the same time, emitting a narrow band beam at a frequency that is the sum of the two incident beams. The intensity of SFG beam, I_{SFGX} , is directly proportional to the square of the second-order polarizability, $P^{(2)}$. The second-order polarizability is induced at the surface by the interaction of the two incident light fields (visible and IR) and the nonlinear second-order effective susceptibility, $\chi_{\text{eff}}^{(2)}$, of the system.

$$I_{\text{SFG}} \propto |P_{\text{eff}}^{(2)}| = \chi_{\text{eff}}^{(2)} : E_{\text{Vis}} E_{\text{IR}} |^2 \quad (1)$$

E_{Vis} and E_{IR} are the electric fields of the visible and IR incident beams at the surface. The second-order effective susceptibility, $\chi_{\text{eff}}^{(2)}$, is separated into two parts, $\chi_{\text{OR}}^{(2)}$ which is the off-resonant susceptibility from the substrate, and $\chi_{\text{R}}^{(2)}$, which is the second-order resonant susceptibility containing the orientation average of the second-order hyperpolarizability of the molecules on the surface, $\langle \beta^{(2)} \rangle$.^{23–27} Both $\chi_{\text{OR}}^{(2)}$ and $\chi_{\text{R}}^{(2)}$ terms are complex quantities, and their phases are interfering with each other.

$$\chi_{\text{eff}}^{(2)} = \chi_{\text{R}}^{(2)} + \chi_{\text{OR}}^{(2)} = \sum_q \frac{N \langle \beta^{(2)} \rangle_q}{\omega_q - \omega_{\text{IR}} - i\Gamma_q} + A_{\text{OR}} e^{i\phi} \quad (2)$$

Here, N is the number of vibrational modes on the surface area contributing to the SFG. ω_q is the resonant frequency of the q th vibrational mode of the molecules on surface. A_{OR} and ρ are the amplitude and phase of the off-resonant susceptibility, respectively. The Lorentzian line shape is used to describe the broadening of the resonant signal caused by time-dependent dephasing and vibration damping and possibly due to the bandwidth of incident beams. Gaussian convolution of eq 2 to account for the inhomogeneity of the surface molecules and the substrates is well-explained in previous papers.^{28,29}

3. EXPERIMENTS

3.1. Materials and Methods. Gold films were prepared by evaporating 99.99% gold (100 nm) on Si(100) wafers precoated with 10 nm of chromium under high vacuum conditions. Octadecanethiol (monodentate molecules) was purchased from Sigma Aldrich, and the preparation of 2-hexadecylpropane-1,3-dithiol (bidentate molecules) has been reported previously.³⁰ Polydimethylsiloxane (PDMS, Sylgard 184, Dow Corning Co.) stamps were prepared by following the manufacturer's instructions.

A drop of the monodentate solution (50 mmol in ethanol) was placed on the PDMS stamp and allowed to dry under a stream of ultrapure nitrogen gas. μCP was then performed by stamping the PDMS block on a freshly prepared gold film for 15 min. After stamping, the gold slide was rinsed with ethanol and dried using a stream of nitrogen gas. The gold film was then immersed in a bidentate SAMs solution (10 mmol in ethanol) for 5 min, washed with ethanol, and then dried under ultrapure nitrogen.

3.2. Optical System. The experimental specifications of the SFGIM technique are well-explained in earlier papers.^{20,28,29,31} The fundamental 1064 nm laser beam and tunable IR are generated by the picosecond Nd:YAG laser (PL2251A, Ekspla). The tunable mid-IR beam from the optical parametric generator/amplifier (OPG/OPA, Laservision) and the 1064 nm pump beam are overlapped spatially and temporally using a copropagating configuration at incident angles of 70 and 60° from the surface normal, respectively. The generated SFG signal is transferred onto a near-IR reflection grating and then subsequently recorded by the intensified CCD camera. The polarization of the incident beams is fixed to p-polarization; therefore, the SFG beam is also p-polarized. The IR beam was continuously tuned from 2800 to 3050 cm^{-1} , and the image was collected at a 5 cm^{-1} interval with a 3000 pulses/image acquisition rate.

3.3. Data Analysis. Images obtained from a CCD camera have a ~ 1 mm field of view with 2 μm resolution. Each pixel corresponds to about 0.8 μm of sample surface. For the data analysis, a 500 \times 500 pixel area at the center of the image stack was used to extract the data set of the 10 \times 10 pixel regions of interest (ROIs). The averaged frequency domain SFG spectra of each ROI are constructed using the ImageJ software with a macro script. Each spectrum has been fitted to Lorentzian line shapes, as shown in eq 2, using Mathematica software. This fitting process of over 2500 individual ROI spectra involves (1) estimation of the initial value through the plot simulation, (2) predetermination of the constraints for each initial parameter, (3) optimization of the iteration numbers for a fitting performance, and (4) reconstruction of the raw images using the fitted value and of amplitude ratio maps for each resonant species to visualize the contrast changes of conformation disorder and local orientation with their distributions. Further

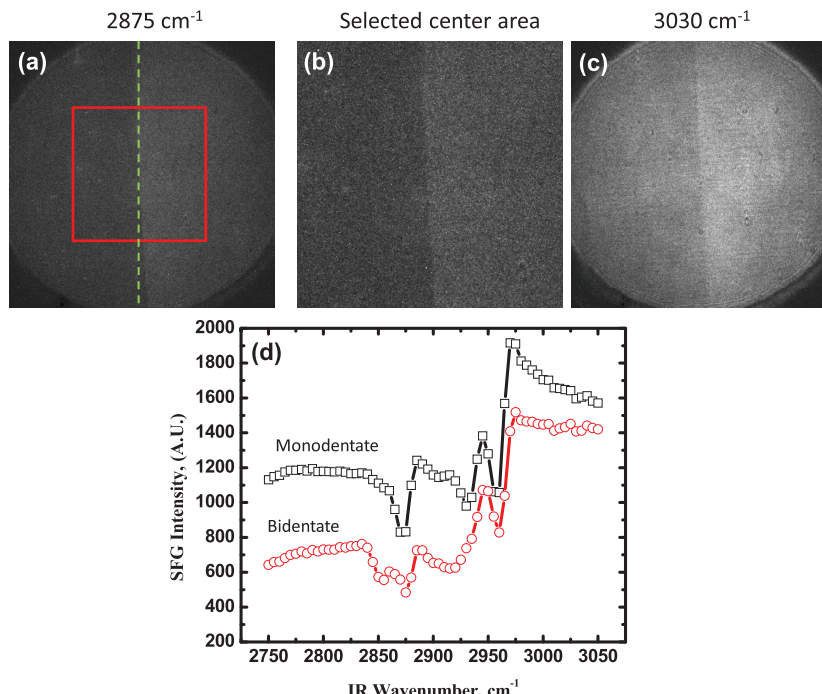


Figure 2. (a) Image taken from SFGIM of a binary system of SAMs on a gold substrate at 2875 cm^{-1} . The left side is the monodentate, and the right side is the bidentate monolayer. (b) Selected center area (500×500 pixels) for analysis at 2875 cm^{-1} of IR wavenumbers. (c) Image taken from SFGIM of a binary system of SAMs on a gold substrate at 3030 cm^{-1} . (d) Average spectra of monodentate (black, square) and bidentate (red, circle) monolayers.

statistical analysis provides quantitative information of the molecular structure on the surface.

4. RESULTS AND DISCUSSION

4.1. Average Spectrum. Figure 2a shows an image at 2875 cm^{-1} taken by SFGIM, and Figure 2b represents the 500×500 pixels of selected area for analysis. The monodentate and bidentate monolayers are on the left and right sides of the substrate image, respectively. Average SFG spectra of each monolayer have been plotted in Figure 2d with an offset of 500 added to each data point of the monodentate spectrum to visually separate it from bidentate spectra. Six resonant vibrations are assigned at 2850 , 2875 , 2905 , 2935 , 2950 , and 2965 cm^{-1} , corresponding the methylene symmetric stretch (d^+), methyl symmetric stretch (r^+), methylene Fermi resonance (d_{FR}^+), methyl Fermi resonance (r_{FR}^+), methyl out-of-plane antisymmetric stretch (r_{op}^-), and methyl in-plane antisymmetric stretch (r_{ip}^-) vibration, respectively.³²

In Figure 2b, a SFGIM image at the r^+ frequency shows a slight contrast change across the borderline of the two monolayers. However, this contrast change does not directly represent the spatial differences in surface monolayer density, conformation, or orientation of the monodentate and bidentate molecules. In fact, some contrast is observed at most IR wavenumbers even when there is no resonance peak observed. Figure 2c represents the raw image extracted from the image stack at 3030 cm^{-1} , where there are no resonant vibrational modes for the SAMs. As shown in Figure 2c, the contrast is observed at most IR wavenumbers regardless of the position of the vibrational resonant signals. It implies that the contrast shown in the image is a result from other factors such as the difference of the monolayer preparation methods, μCP for the monodentate and backfilled for the bidentate monolayer. Thus, it is required that a chemical map be generated by interpreting

the stack of images in order to understand the surface characteristics. A custom-built program using Mathematica software is employed to reconstruct the chemical map of the selected area (500×500 pixels) and interpret the sample surface from ROI fit results.

4.2. Conformation Disorder. When alkyl chains attach on the surface and form a perfect all-trans conformation, it is considered that the CH_2 vibration dipoles will cancel each other and will not show any SFG resonant intensity due to the inversion symmetry in the alkyl chains.^{25,33} However, in the presence of conformation disorder (i.e., a gauche defect), it breaks the inversion symmetry on the alkyl chain and develops SFG intensity from CH_2 vibrational modes. Thus, the degree of conformation disorder of the SAMs can be determined from the observed amplitude of d^+ and d_{FR}^+ vibrational modes.

The conformation disorder of monodentate and bidentate monolayers is well presented in the averaged spectra, as shown in Figure 2d. Both resonant peaks (which appear as negative due to the phase effect) appeared in SFG spectra of bidentate SAMs. Although the SFG resonant signals of the d_{FR}^+ vibrational modes at $\sim 2905\text{ cm}^{-1}$ are partially overlapped with other resonant signals, d^+ vibrational modes are well-separated from others and clearly exhibit a resonant peak at $\sim 2850\text{ cm}^{-1}$. In order to quantify the degree of conformation disorder in each ROI, the resonant peak intensity changes due to the number of vibrational modes presented in each ROI (inhomogeneity of the SAMs) need to be considered. To compensate for the inhomogeneity on the monolayers, the conformation disorder is examined by the amplitude ratio of d^+ and r^+ vibrations (conformation ratio, d^+/r^+).^{27,34} Thus, the SAMs molecules that possess more conformation order show a lower value of the conformation ratio, d^+/r^+ . The degree of conformation order in each ROI is extracted from the ROI fitting results and reconstructed into a conformation map, as shown in Figure 3a.

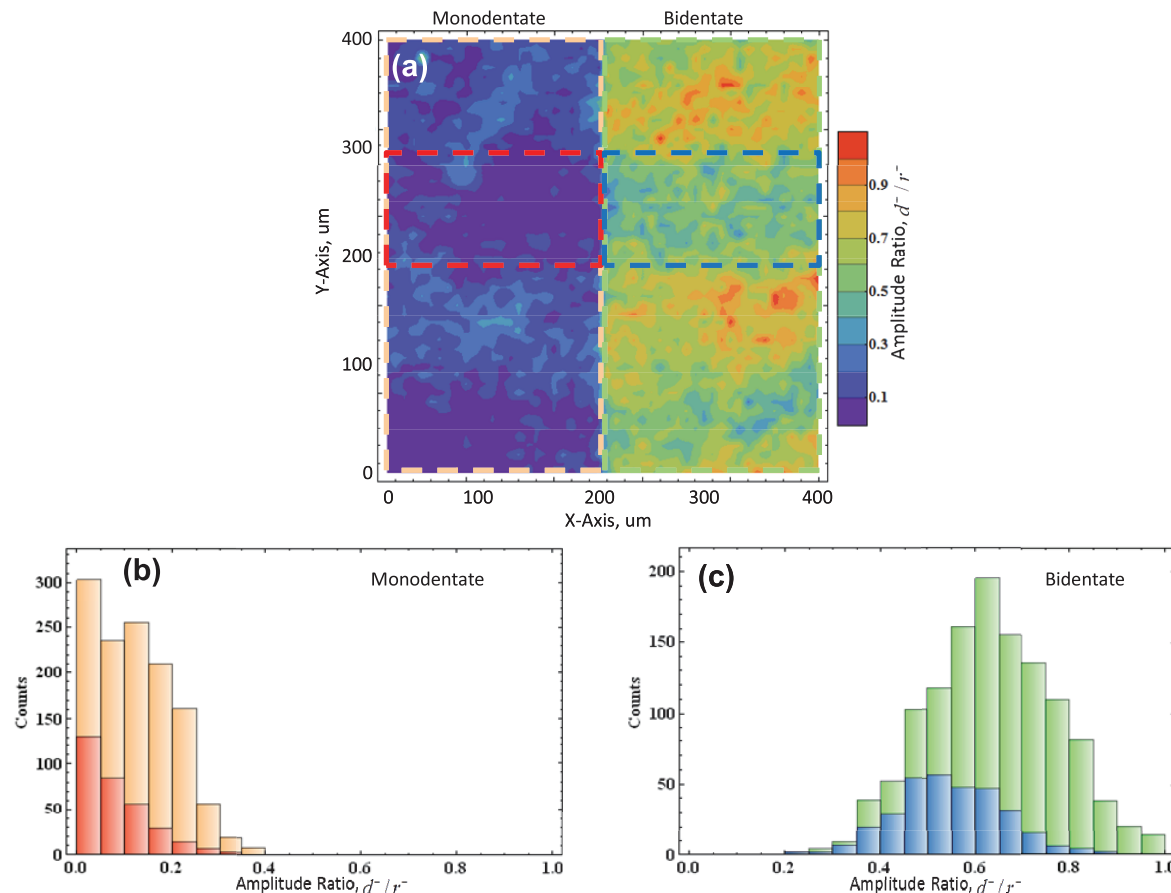


Figure 3. (a) Reconstructed map of the amplitude ratio of d^+ and r^- extracted from all of the ROI fitting results. The left side is the monodentate, and the right side is the bidentate monolayer. (b) Histogram of the amplitude ratio of d^+ and r^- in the monodentate area. The subset (red) shows a histogram generated from the inside of the red dashed line box in the reconstructed map. (c) Histogram of the amplitude ratio of d^+ and r^- in the bidentate area. The subset (blue) shows the histogram generated from the inside of the blue dashed line box in the reconstructed map.

The left side (orange dashed line) and right side (green dashed line) of the conformation map denote monodentate and bidentate monolayers, respectively. Figure 3b and c shows the histogram of the conformation ratio, d^+ / r^- . The subset (red and blue) of each histogram is generated from inside of the red dashed line and blue dashed line in the reconstructed map, showing that the conformation order of the SAMs is not unique but exhibits variations across the substrate.

The spatial contrast of the monolayer conformation map and the histograms shows several features. First, it shows the influence of the SAMs head group on the monolayer formation. The conformation ratio of d^+ / r^- on the monodentate monolayer (orange dashed line in Figure 3a) ranges from 0 to 0.3. As mentioned before, the conformation ratio, d^+ / r^- is related to the degree of conformation disorder in the SAMs molecules. Therefore, the result implies that most of the alkyl chains in the monodentate monolayer prefer to form an all-trans structure. On the other hand, the ratio on the bidentate monolayer (green dashed line in Figure 3a) is distributed from 0.3 to 0.9, which indicates the relatively large degree of conformation disorder in the bidentate monolayer. These results are well-matched with the simulation and those in previous observations.^{22,35} The orange and green histogram shown in Figure 3b and c present a distribution of the conformation ratio, d^+ / r^- , in the monodentate and bidentate monolayers, respectively. The statistical parameters obtained from the histograms are listed in Table 1. The median value of

Table 1. Statistical Parameters of the Histogram of the Conformation Ratio, d^+ / r^- , in Each SAM

	total monolayer (orange and green)			inset monolayer (red and blue)		
	mean	median	standard deviation	mean	median	standard deviation
monodentate	0.12	0.12	0.09	0.08	0.07	0.07
bidentate	0.64	0.63	0.14	0.55	0.54	0.11

the conformation ratio in the monodentate monolayer is 0.12, and that for the bidentate monolayer is 0.63, which suggests that there is more conformation disorder occurring in the bidentate monolayer on the gold substrate.²²

The spatial contrasts shown in the reconstructed ratio map in Figure 3a also represent the local conformation disorder of the SAMs, which are possibly affected by the homogeneity of the substrate. This spatial contrast shows dramatic change in monodentate SAMs, which is inside of the orange dashed line of Figure 3a. The orange colored histogram in Figure 3b indicates the distribution of the conformation disorder in monodentate SAMs, and the red colored one represents the distribution inside of the red rectangle in Figure 3a. While the distribution from the orange colored histogram shows its median at 0.12, the red colored one shows the median at 0.07, as shown in Table 1. The large difference between the medians

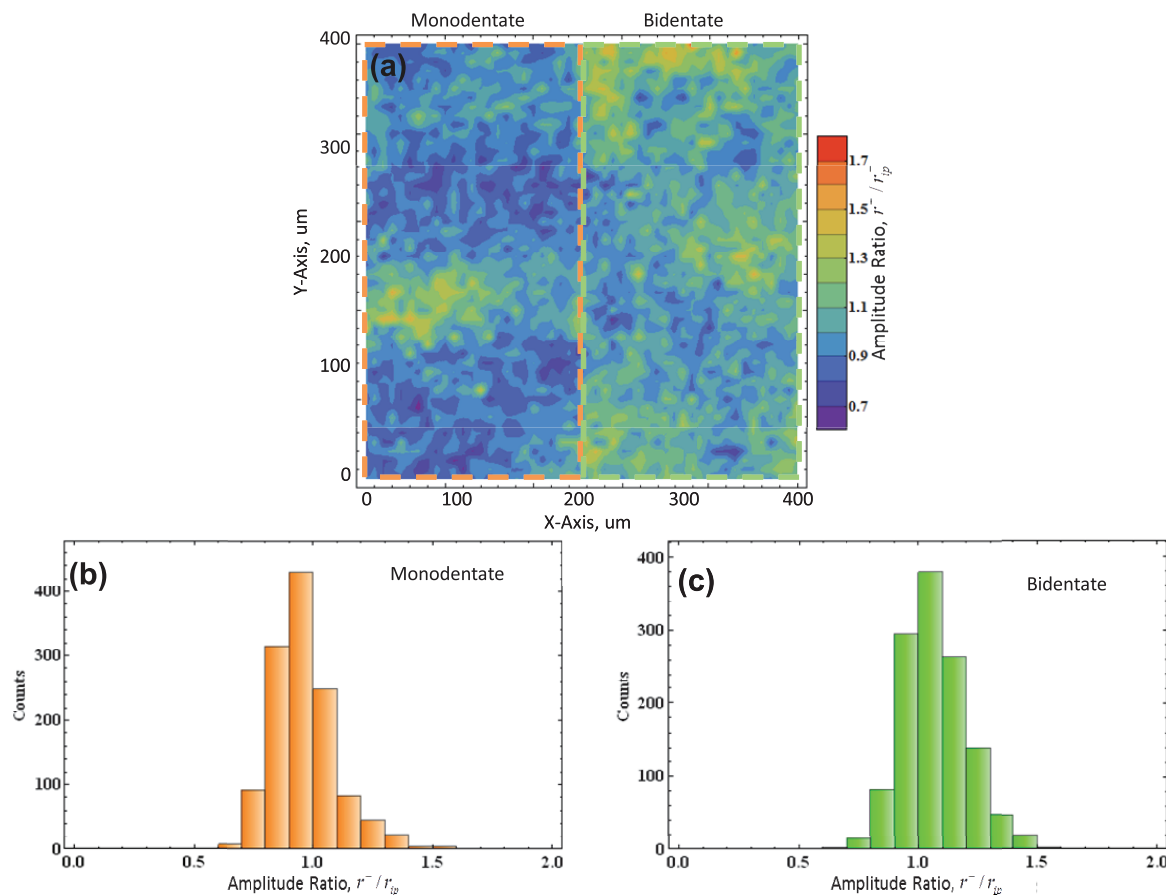


Figure 4. (a) Reconstructed map of the amplitude ratio of r^+ / r_{ip}^- extracted from all of the ROI fitting results. The left side is the monodentate, and the right side is the bidentate monolayer. (b) Histogram of the amplitude ratio of r^+ / r_{ip}^- in the monodentate area. (c) Histogram of the amplitude ratio of r^+ / r_{ip}^- in the bidentate area.

of the two histograms indicates that the monodentate SAMs are highly sensitive to the monolayer homogeneity.

The degree of conformation disorder in bidentate SAMs also appears to be sensitive to the homogeneity. The green and blue histograms shown in Figure 3c present the distribution of the conformation ratio, d^+ / r^+ , generated from the inside of the green dashed line and blue dashed line, respectively. The conformation ratio, d^+ / r^+ , which shows median of 0.54 for the blue histogram from inside of the blue dashed line, exhibits substantial change from the median value, 0.63, as observed from the total bidentate monolayer histogram. The results represent that the monolayer inhomogeneity significantly affects the conformation order on both SAMs.

4.3. Orientation. The orientation analysis in SFG is based on the observation of two orthogonal sets of resonant effective susceptibilities, $\chi_R^{(2)}$. The mathematical formulation for the relation between the orientation angle of the surface molecules and the measurable $\chi_R^{(2)}$ is well-established elsewhere.^{22,26,28,29,36,37} Assuming that the surface is isotropic, previous studies show that $\chi_R^{(2)}$ is expressed as a linear combination of $\langle \cos \theta \rangle$ and $\langle \cos^3 \theta \rangle$, where θ is the tilt angle of a methyl terminal group in the alkyl chain from surface normal and $\langle \rangle$ represents the orientational average.^{26,38–41} The coefficients of the each cosine term consist of the hyperpolarizability tensor elements, $\beta_{ijk}^{(2)}$, of the methyl group molecular vibrational mode. The ratio of $\beta_{ijk}^{(2)}$ involved in symmetric and antisymmetric methyl group vibration is readily obtained from the Raman depolarization ratio.^{36,37} Thus, by

taking the SFG amplitude ratio of r^+ and r_{ip}^- vibrational modes, the average orientation tilt angles, θ , are deduced. It is to be noted that for the conventional SFG technique without spatial resolution, the orientational distribution is treated as a δ -function distribution. Several studies use a Gaussian function to convolute the orientation curve and to approximate the orientational angle at various distributions.^{42–45} However, in SFGIM, the δ -function distribution approximated θ is calculated first from each ROI, and then, the list of all of the averaged θ 's from each ROI shows a distribution that describes the orientational distribution and homogeneity of the monolayer.

In order to determine the orientation of the monodentate and bidentate molecules on the surface, amplitude ratios of r^+ and r_{ip}^- vibration resonance (orientation ratio, $a \times r^+ / r_{ip}^-$) have been calculated from each ROI, and the orientation contour map is reconstructed as shown in Figure 4a. A constant in the orientation ratio, $a = 1.33$, is a correction factor that takes into account the Fermi interaction in r^+ and r_{FR}^+ .³⁷

The left side (orange dashed line) and right side (green dashed line) of the orientation map in Figure 4a represent the monodentate and bidentate SAMs on the gold surface, respectively. In contrast to the well-defined boundary between the monodentate and bidentate SAMs that appeared in the conformation map (in Figure 3), the orientation map does not show a contrast variation between the two SAM regions. It suggests that the orientational tilt angle of the methyl terminal group is not sensitive to the number or size of the head groups

in this system. The statistics of the orientation ratio also support this observation. The histogram in Figure 4a and b shows the distribution of the orientation ratio for monodentate and bidentate monolayers, respectively, and the statistical parameters are listed in Table 2. The statistical median of the

Table 2. Statistical Parameters of the Histogram of the Orientation Ratio, r^+/r_{ip}^- , in Each SAM

	mean	median	standard deviation
monodentate	0.96	0.94	0.13
bidentate	1.07	1.06	0.14

histogram, which is 0.94 for the monodentate, is only somewhat different from the median of 1.06 for the bidentate monolayer. In addition, the shape of the histogram in Figure 4b and c and the standard deviation of each histogram listed in Table 2 are also nearly identical in both SAMs. These results support that the variation of the head group of the SAM molecule does not affect the average orientation angle on the gold surface in this system.

4.4. Tilt Angle Analysis. Here, each ROI ($10 \times 10 \text{ }\mu\text{m}$ area) is treated as a δ -function distribution to convert the orientation ratio to the tilt angle of the surface molecules. This δ -function distribution approximation by using small ROIs in processing images obtained from SFGIM is established in a previous study.²⁸ Figure 5 illustrates the simulated orientation

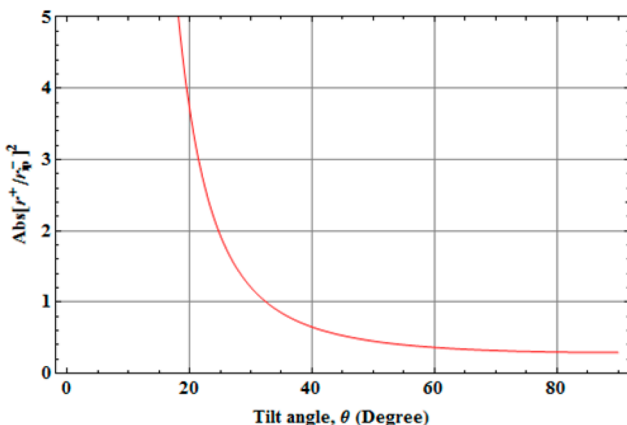


Figure 5. Simulated orientation curve for the methyl terminal group in the alkyl chain. The plot shows the orientation intensity ratio, $|r^+/r_{ip}^-|^2$, changes as a function of the tilt angle of the methyl group.

curve with the δ -function distribution for the methyl terminal group in the alkyl chain. The orientation curve shows that the orientation intensity ratio, $|r^+/r_{ip}^-|^2$, changes as a function of the tilt angle of the methyl group.^{22,29} The intensity ratio, $|r^+/r_{ip}^-|^2$, obtained from Figure 4 has been converted to the corresponding methyl tilt angle by the simulated orientation curve. The resulting histograms of the orientation distributions for monodentate and bidentate monolayers are depicted in Figure 6a and b, respectively. The histograms of each monolayer have been fitted into a normal distribution (red solid line) and skew normal distribution (blue solid line), and the resulting statistical values are listed in Table 3. Both monolayers show relatively good homogeneity with a quite narrow distribution, the interquartile ranges ($2 \times$ quartile deviation, containing 50% of the distribution). The monodentate monolayer shows a slightly wider distribution than that

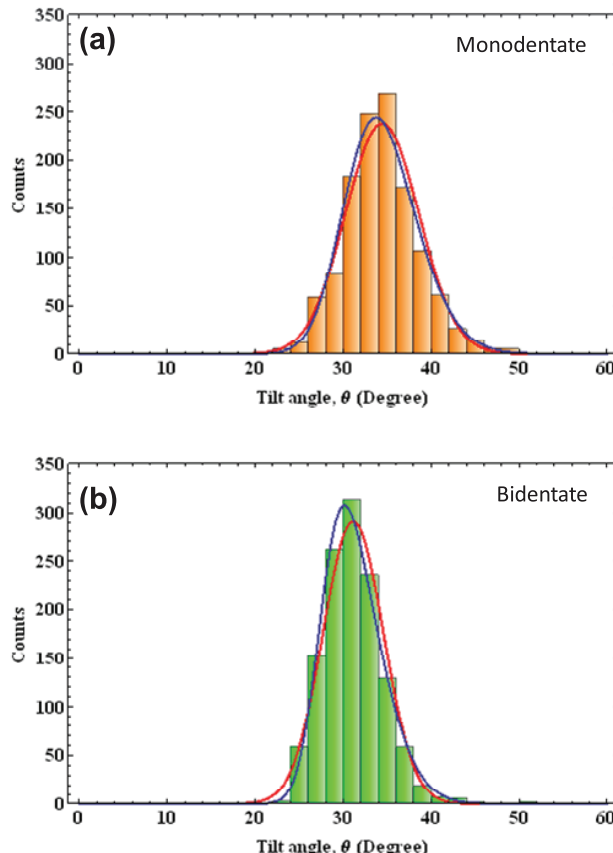


Figure 6. (a) Histogram of the tilt angle of the r^+ vibration vector in the monodentate area. (b) Histogram of the tilt angle of the r^+ vibration vector in the bidentate area. Each histogram has been fitted with a normal distribution (red) and a skew normal distribution (blue).

of the bidentate, as shown in Table 3. The histogram of the monodentate monolayer exhibits small asymmetry with the skewness estimated to be 0.4, while the bidentate monolayer shows a higher degree of asymmetry in the orientation distribution with a positive skewness of 0.8. The slight difference in distribution and skewness of the two SAMs is mainly due to the nonlinear relationship between the tilt angle and intensity ratio, as shown in Figure 5. As expected from the orientation ratio analysis, both the monodentate and bidentate show similar average orientation angles of 31 and 34°.

These observations from the orientation ratio analysis and the deduced tilt angle of the monodentate and bidentate SAMs exhibit differences from the previous observation, where the average orientation of the multidentate monolayers changes substantially from that of the monodentate monolayer.²² However, analytical errors are found in the previous report; the ratio of 0.85 deduced from the monodentate (octadecane-thiol) monolayer in ref 22 was analyzed using a five resonant peak SFG fitting model without the r_{op}^- vibrational mode. On the other hand, bidentate and tridentate monolayers were fitted using a six peak SFG model, and ratios of 0.36 and 0.32 were estimated from the fitting results. The loss of consistency in the fitting process is critical and results in misunderstanding of the interfacial characteristics, even though the amplitude of the r_{op}^- vibrational mode was not used to interpret the surface molecular orientation. This is important because the overall spectral intensity is governed by the interference between the

Table 3. Statistical Parameters of the Histogram of the Tilt Angle of the r^+ Vibration Vector in Each SAM

	normal distribution		skew normal distribution				
	mean (°)	standard deviation (°)	median (°)	quartile deviation (°)	skewness (°)	lower quartile (°)	upper quartile (°)
monodentate	34	4.2	34	2.6	0.4	32	37
bidentate	31	3.4	31	2.2	0.8	29	33

resonant signals. As a result, the orientation ratio from the five resonant peak SFG fitting model shows a much larger value than the ratio from the six resonant peak SFG fitting model. On the other hand, the orientation ratios of the bidentate and tridentate, which are fitted by the same SFG model, are close to each other. The data in ref 22 have been acquired and reanalyzed with consistent peak assignments and better fitting parameters, as described in this paper. The fitting results (see the Supporting Information) show that there are no significant differences in the statistical medians for the orientation ratio between monodentate (0.88) and bidentate (0.90) SAMs.

4.5. Surface Molecule Density. As shown in eq 2, the peak amplitude is proportional to the number of vibrational modes on the surface. The monodentate and bidentate molecules contain one methyl terminal group per molecule. Therefore, the amplitude of r^+ is proportionally related to a density of the SAMs on the surface. The amplitude of r^+ in each ROI generally increases with the number of molecules, assuming that the SAMs in all of the ROIs have identical orientations.

However, all of the molecules on a surface do not have a unique orientational angle but show an orientational distribution. In addition, several studies show that the large orientational distribution significantly decreases the peak amplitude.^{22,28,29} Thus, the monolayer density estimated from the peak amplitude has a limitation such that the amplitude is also a function of the tilt orientation and distribution as well as the density of the vibrational modes, as shown in eq 2. In order to estimate the effect of orientation, distribution, and surface density on the SFG amplitude, the amplitude changes of the r^+ vibrational mode relative to the number of vibrational modes, N , and orientational distribution, σ , are simulated at a 33° tilt angle and are illustrated in Figure 7. The simulated plots (a) and (b) show the normalized amplitude of the r^+ vibrational mode as a function of the orientational distribution, σ , and as a function of the surface density, respectively. The amplitude is normalized at the zero tilt angle, zero distribution, and full coverage of the surface molecule density. If r^+ has a wide orientational distribution around the average tilt angle, the SFG resonance intensity decreases. Therefore, estimation of the molecule density from the amplitude of r^+ without consideration of the orientational distribution is generally not applicable in SFG techniques.

SFGIM techniques, however, can possibly deduce the orientational distribution of SAMs on the surface. The tilt angle distribution obtained by the orientational analysis in this paper shows a narrow standard deviation of 4.2 for the monodentate and 3.4 for the bidentate monolayer with an average tilt angle of 33° , as shown in Table 3. On the basis of the orientation distribution without consideration of the packing density and the average tilt angle, the r^+ resonant amplitude ratio of bidentate to monodentate is calculated.

Figure 8 shows simulated SFG intensity changes of r^+ resonance as a function of its orientation distribution at an average tilt angle of 33° . The simulated SFG intensities of 7.077 and 7.080 are calculated from the distribution angle standard

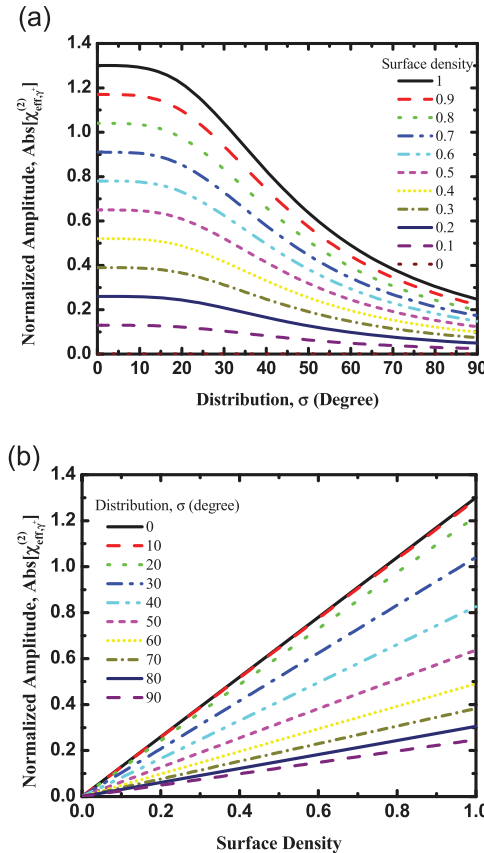


Figure 7. Normalized amplitude of the r^+ vibrational mode at a 33° methyl tilt angle as a function of (a) the orientational distribution, σ , and (b) the surface density. The amplitude is normalized at zero tilt angle, zero distribution, and full coverage of the surface molecule density.

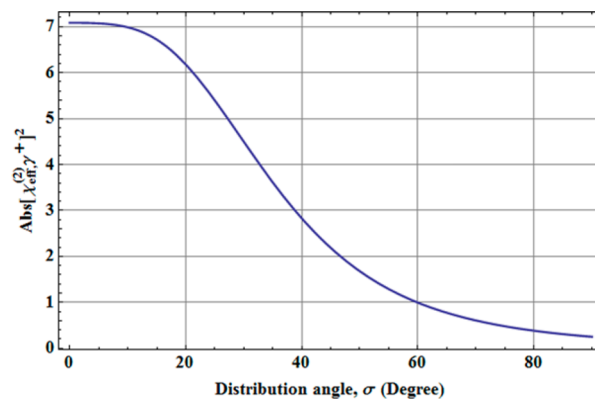


Figure 8. Simulated SFG intensity changes of the r^+ resonance as a function of its orientation distribution at an average tilt angle of 33° .

deviations of 4.2 and 3.4 observed in the experiments for monodentate and bidentate monolayers, respectively. The corresponding amplitude ratio due to the difference in the orientation distributions is deduced to be ~ 1 , indicating that

the differences of the r^+ resonant amplitude that occurred from monodentate and bidentate SAMs are negligible. Thus, it is permissible to consider that the amplitude of the r^+ vibrational mode mostly depends on the density of the SAMs molecules on the surface, in this case precluding the orientation distribution. Hence, the estimated resonant amplitude of the r^+ vibration is considered to represent the surface molecule density in each ROI.

In order to visualize the monodentate and bidentate SAMs on the surface, the amplitude of r^+ estimated from fitting analysis was reconstructed as a contour map in Figure 9. The

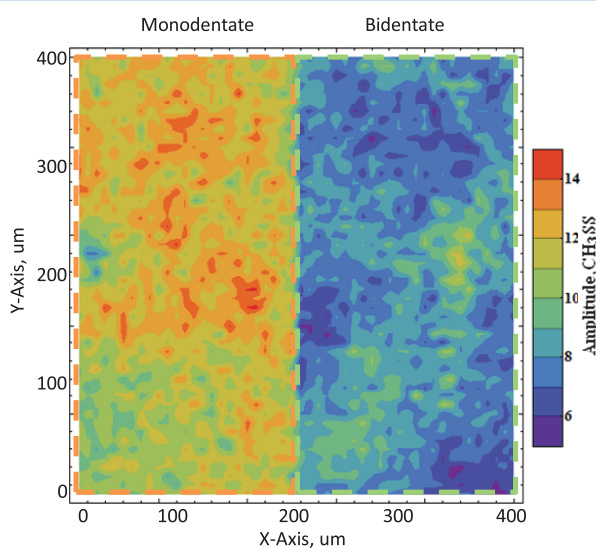


Figure 9. Reconstructed contour map of the amplitude of the r^+ vibration estimated from fitting analysis. The left and right sides of the amplitude map correspond to the monodentate and bidentate monolayers.

left and right sides of the map correspond to the monodentate and bidentate monolayers, respectively. In comparison with the SFGIM image at the r^+ vibrational mode frequency (2875 cm^{-1}) depicted in Figure 2b, the amplitude map shows great improvement in contrast, which is relevant to the local surface density of the SAMs.

From the contour map of the r^+ resonant amplitude in Figure 9, the average amplitudes of the monodentate (orange dashed line) and bidentate (green dashed line) monolayers are calculated to be 11.5 and 8.0, respectively, as shown in Table 4. From the average amplitude of each monolayer, it is

Table 4. Statistical Parameters of the Histogram of the Reconstructed Contour Map of Amplitude of the r^+ Resonance Estimated from Fitting Analysis in Each SAM

	mean	median	standard deviation	ratio (bidentate/monodentate)
monodentate	11.5	11.6	1.1	0.7
bidentate	8.0	7.9	1.0	

estimated that the surface molecule density ratio of the bidentate to monodentate monolayer is 0.7. A previous photoelectron spectroscopy study also reported a reduction of 35% surface monolayer density for the bidentate and 49% for the tridentate SAMs due to the size of the head group.³⁰ The low surface coverage in bidentate SAMs provides a flexibility for the molecules to form conformation disorder, as observed from

the conformation disorder analysis in Figure 3, and to exhibit a wide orientational distribution, as observed from the orientation tilt angle analysis in Figure 6.

Generally, it is well-known that the monodentate SAMs are densely packed on the gold surface.^{46–49} The alkanethiols on a single-crystal Au(111) surface present a lattice structure of $(\sqrt{3} \times \sqrt{3})R30^\circ$.^{47,50} However, evaporated gold surfaces on silicon wafers are polycrystalline and typically show gold crystal domains that are on the order of several hundred nanometers.⁹ This heterogeneity occurring from evaporated polycrystalline or pseudo-single-crystal gold surfaces greatly impacts the homogeneity of SAMs and generates defects.² In this aspect, the amplitude map in Figure 9 also provides a good estimation of the surface SAMs density depending on the substrate heterogeneity. The local variations on the surface are correlated to the conformation disorder and the orientation angle across the substrate, as shown in Figures 3 and 4. For example, in monodentate SAMs, the upper area in Figure 9 exhibits a higher amplitude, and this area corresponds to the inside of the red dashed line in the conformation map (Figure 3a). The detailed correlation between each characteristic map is examined in scatter plots.

4.6. Scatter Plot. Mapping analysis shows that surface characteristics such as the degree of conformation disorder, surface orientation of the SAMs, and relative surface molecule density depend on the local homogeneity of the gold substrate and the number of head groups in SAM molecules. Moreover, while the tilt angle remains almost the same, it is observed that the molecular density and degree of conformation disorder of SAMs with the bidentate head group are greatly varied compared with those of monodentate SAMs. In addition to each characteristic map of the surface monolayer, correspondences among the surface characteristics have been investigated.

The degree of conformation disorder has been plotted against the surface packing density represented by the amplitude of the r^+ vibrational mode, as shown in Figure 10a. Each point depicted in the orange and green colors corresponds to the ROIs of the monodentate and bidentate monolayers, respectively. The ellipsoidal lines contain 95.4% confidence ranges of each scatter plot. As shown in Figure 10a, the degree of the conformation ratio in the bidentate monolayer highly depends on the surface monolayer density; a high conformation ratio appears in the lower amplitude of the r^+ vibrational mode, which means that the loosely packed monolayer area exhibits more gauche defects.⁵¹ The occurrence of conformation disorder in monodentate SAMs does not reveal strong correspondence, as shown in the orange colored scatterplot in Figure 10a, and most of the molecules in the monodentate SAMs are well-organized without conformation disorder.

The tilt angle variance from its median value also has been plotted against the surface packing density represented by the amplitude of the r^+ vibrational mode, as shown in Figure 10b. The tilt angle variance shows low correspondence on the surface packing density in both monodentate (orange colored) and bidentate (green colored) monolayers. The terminal methyl group tends to form a higher orientation angle (far away from the surface normal) at lower surface packing density.

In addition, the scatter plot of the conformation ratio against the tilt angle variance from the median value is presented in Figure 10c. The correspondence of the conformation ratio to the tilt angle variance of the monodentate monolayer (orange colored) is similar to the amplitude of the r^+ vibrational mode shown in Figure 10a. For the bidentate monolayer, even though

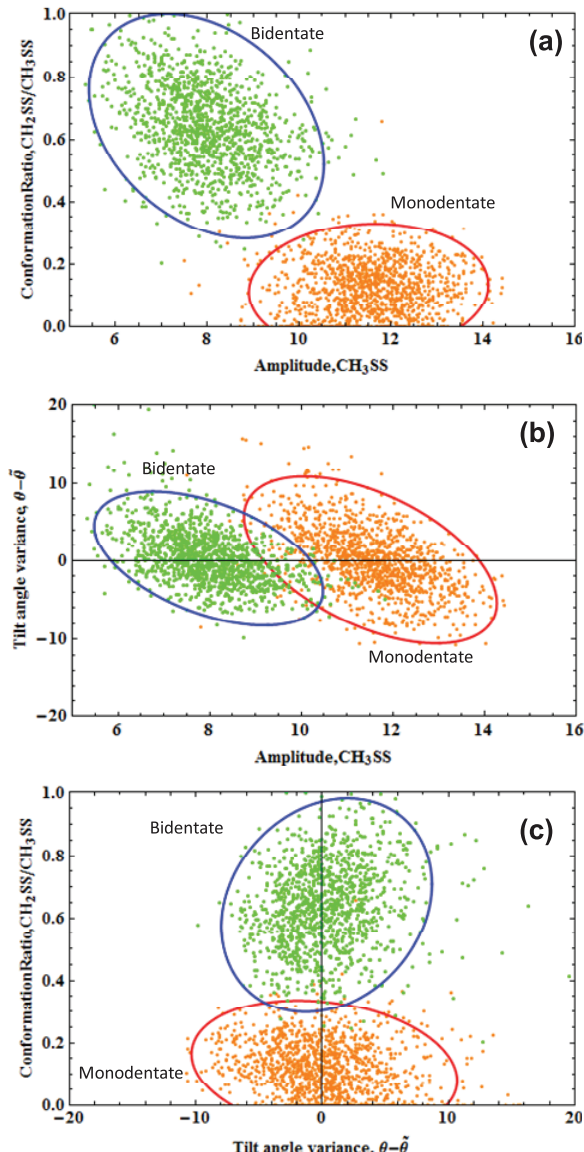


Figure 10. (a) Scatter plot of the degree of conformation disorder against the amplitude of the r^+ vibrational mode. (b) Scatter plot of the tilt angle variance from its media value against the amplitude of the r^+ vibrational mode. (c) Scatter plot of the conformation ratio against the tilt angle variance. Each point depicted in the orange and green color corresponds to the monodentate and bidentate monolayers, respectively. The ellipsoidal lines contain 95.4% confidence ranges of each scatter plot.

the conformation disorder shows large correspondence to the surface packing density in Figure 10a, it appears that there is no perceptible relation between the conformation ratio and tilt angle variance, as shown in Figure 10c. It is due to the degree of conformation disorder in bidentate SAMs being dominantly controlled by the molecular spacing introduced from the large head group, unlike that in monodentate SAMs where it is influenced by the heterogeneity of the substrate.

4.7. Surface Structure. From the orientation map in Figure 9, it was found that the conformation disorder is more dominant on the bidentate monolayer. When there is a conformation disorder such as a gauche defect, it is expected for the tilt angle of the r^+ vibration dipole vector to be shifted far from the most preferential angle, which is about 30° .^{8,27}

However, orientation analysis suggests similar tilt angles of 34 and 31° for monodentate and bidentate SAMs, respectively. The SAMs molecular structures on the gold surface based on the methyl group angle and gauche defects observed in this study are made. It is generally known that the surface molecules form a well-ordered and densely packed monolayer when the alkyl chain is arranged in an all-trans configuration, exhibiting a narrow distribution. However, due to the size of the head group in bidentate monolayers, the large spacing between the alkyl chains is introduced at the near surface. Due to this, it is expected to have the gauche defect close to the gold substrate, as expected in theoretical simulations reported.³⁵ Also the neighboring alkyl chain provides reinforcement by means of a van der Waals interaction for the C–C backbone to be in the preferential orientation, which results in a similar orientation angle as the monodentate monolayer.

5. SUMMARY

In this study, a binary system of monodentate and bidentate molecules on a gold substrate has been analyzed using spatially resolved SFGIM. An analytical process of the images collected from SFGIM has been demonstrated. The reconstruction map of r^+ vibrational mode amplitudes shows local variations of packing density due to the substrate homogeneity. The relative ratio of the surface packing density of the bidentate and monodentate monolayers is estimated to be 0.7 from the amplitude map. The loosely packed density in the bidentate monolayer is a consequence of the large head group that introduces spaces between the molecules on the surface. The low surface density of the bidentate molecules leads to the significant degree of conformation disorder in the alkyl chains. It is, however, found that the monodentate monolayer possesses trivial conformation disorder localized at heterogeneous substrate. Despite the significant degree of conformation disorder observed, the average methyl tilt angle of 31° in the bidentate monolayer is almost the same as that in the monodentate monolayer. It suggests that the conformation disorder in the bidentate molecule occurs near the gold substrate, and the neighboring alkyl chain provides reinforcement by van der Waals interaction for the alkyl chain to be in the preferential orientation. An asymmetric and wide distribution of tilt angles in the bidentate monolayer implies that wider spacing between the molecules in the bidentate monolayer allows the alkyl chain to orient more freely. Correspondences among the surface packing density, degree of conformation disorder, and CH_3 tilt angle variance of each monodentate and bidentate SAM have been investigated by scattered plots. It is found that the degree of conformation disorder in bidentate SAMs is dominantly controlled by the molecular spacing introduced from the large head group, unlike in monodentate SAMs where it is influenced by the heterogeneity of the substrate.

■ ASSOCIATED CONTENT

S Supporting Information

A custom-built program using Mathematica software to determine the suitable constraint ranges for fitting each ROI, mathematical formulation for orientation analysis, a list of constraints and initial parameters used for the ROI fitting of the SFG data from ref 1, and orientation analysis of the SFG data from ref 1. This material is available free of charge via the Internet at <http://pubs.acs.org>.

AUTHOR INFORMATION

Corresponding Author

*E-mail: sbaldelli@uh.edu. Telephone: 1-832-842-8844. Fax: 1-713-743-2709.

Notes

The authors declare no competing financial interest.

ACKNOWLEDGMENTS

We thank the National Science Foundation (DMR-0856009 (S.B.) and DMR-0906727 (T.R.L.)), the Robert A. Welch Foundation (E-1320), and the Texas Center for Superconductivity at the University of Houston for generous financial support.

REFERENCES

- (1) Laibinis, P. E.; Whitesides, G. M.; Allara, D. L.; Tao, Y. T.; Parikh, A. N.; Nuzzo, R. G. Comparison of the Structures and Wetting Properties of Self-Assembled Monolayers of *n*-Alkanethiols on the Coinage Metal Surfaces, Cu, Ag, Au. *J. Am. Chem. Soc.* **1991**, *113*, 7152–7167.
- (2) Love, J. C.; Estroff, L. A.; Kriebel, J. K.; Nuzzo, R. G.; Whitesides, G. M. Self-Assembled Monolayers of Thiolates on Metals As a Form of Nanotechnology. *Chem. Rev.* **2005**, *105*, 1103–1169.
- (3) Xia, Y.; Whitesides, G. M. Soft Lithography. *Annu. Rev. Mater. Sci.* **1998**, *28*, 153–184.
- (4) Lavrich, D. J.; Wetterer, S. M.; Bernasek, S. L.; Scoles, G. Physisorption and Chemisorption of Alkanethiols and Alkyl Sulfides on Au(111). *J. Phys. Chem. B* **1998**, *102*, 3456–3465.
- (5) Schreiber, F. Structure and Growth of Self-Assembling Monolayers. *Prog. Surf. Sci.* **2000**, *65*, 151–257.
- (6) Schwartz, D. K. Mechanisms and Kinetics of Self-Assembled Monolayer Formation. *Annu. Rev. Phys. Chem.* **2001**, *52*, 107–137.
- (7) Bain, C. D.; Troughton, E. B.; Tao, Y. T.; Evall, J.; Whitesides, G. M.; Nuzzo, R. G. Formation of Monolayer Films by the Spontaneous Assembly of Organic Thiols from Solution onto Gold. *J. Am. Chem. Soc.* **1989**, *111*, 321–335.
- (8) Dubois, L. H.; Nuzzo, R. G. Synthesis, Structure, and Properties of Model Organic Surfaces. *Annu. Rev. Phys. Chem.* **1992**, *43*, 437–463.
- (9) Goutev, N.; Futamata, M. Attenuated Total Reflection Surface-Enhanced Infrared Absorption Spectroscopy of Carboxyl Terminated Self-Assembled Monolayers on Gold. *Appl. Spectrosc.* **2003**, *57*, 506–513.
- (10) Bryant, M. A.; Pemberton, J. E. Surface Raman Scattering of Self-Assembled Monolayers Formed from 1-Alkanethiols at Silver Electrodes. *J. Am. Chem. Soc.* **1991**, *113*, 3629–3637.
- (11) Bryant, M. A.; Pemberton, J. E. Surface Raman Scattering of Self-Assembled Monolayers Formed from 1-Alkanethiols: Behavior of Films at Gold and Comparison to Films at Silver. *J. Am. Chem. Soc.* **1991**, *113*, 8284–8293.
- (12) Orendorff, C. J.; Gole, A.; Sau, T. K.; Murphy, C. J. Surface-Enhanced Raman Spectroscopy of Self-Assembled Monolayers: Sandwich Architecture and Nanoparticle Shape Dependence. *Anal. Chem.* **2005**, *77*, 3261–3266.
- (13) Eisert, F.; Dannenberger, O.; Buck, M. Molecular Orientation Determined by Second-Harmonic Generation: Self-Assembled Monolayers. *Phys. Rev. B* **1998**, *58*, 10860–10870.
- (14) Cai, X.; Baldelli, S. Surface Barrier Properties of Self-Assembled Monolayers as Deduced by Sum Frequency Generation Spectroscopy and Electrochemistry. *J. Phys. Chem. C* **2011**, *115*, 19178–19189.
- (15) Jacob, J. D. C.; Rittikulittichai, S.; Lee, T. R.; Baldelli, S. Characterization of Sams Derived from Octadecyloxyphenylethane-thiols by Sum Frequency Generation. *J. Phys. Chem. C* **2013**, *117*, 9355–9365.
- (16) Giancarlo, L. C.; Flynn, G. W. Scanning Tunneling and Atomic Force Microscopy Probes of Self-Assembled, Physisorbed Monolayers: Peeking at the Peaks. *Annu. Rev. Phys. Chem.* **1998**, *49*, 297–336.
- (17) Xia, Y.; Whitesides, G. M. Soft Lithography. *Angew. Chem., Int. Ed.* **1998**, *37*, 550–575.
- (18) Wolfe, D. B.; Love, J. C.; Paul, K. E.; Chabinyc, M. L.; Whitesides, G. M. Fabrication of Palladium-Based Microelectronic Devices by Microcontact Printing. *Appl. Phys. Lett.* **2002**, *80*, 2222–2224.
- (19) Cimatu, K. A.; Baldelli, S. Chemical Microscopy of Surfaces by Sum Frequency Generation Imaging. *J. Phys. Chem. C* **2009**, *113*, 16575–16588.
- (20) Cimatu, K.; Baldelli, S. Sum Frequency Generation Microscopy of Microcontact-Printed Mixed Self-Assembled Monolayers. *J. Phys. Chem. B* **2006**, *110*, 1807–1813.
- (21) Cimatu, K.; Moore, H. J.; Barriet, D.; Chinwangso, P.; Lee, T. R.; Baldelli, S. Sum Frequency Generation Imaging Microscopy of Patterned Self-Assembled Monolayers with Terminal –CH₃, –OCH₃, –CF₂CF₃, –C=C, –Phenyl, and –Cyclopropyl Groups. *J. Phys. Chem. C* **2008**, *112*, 14529–14537.
- (22) Hernandez, M.; Chinwangso, P.; Cimatu, K.; Srisombat, L.-O.; Lee, T. R.; Baldelli, S. Chemical Imaging and Distribution Analysis of Mono-, Bi-, and Tridentate Alkanethiol Self-Assembled Monolayers on Gold by Sum Frequency Generation Imaging Microscopy. *J. Phys. Chem. C* **2011**, *115*, 4688–4695.
- (23) Zhu, X. D.; Suhr, H.; Shen, Y. R. Surface Vibrational Spectroscopy by Infrared–Visible Sum Frequency Generation. *Phys. Rev. B* **1987**, *35*, 3047–3050.
- (24) Bain, C. D. Sum-Frequency Vibrational Spectroscopy of the Solid–Liquid Interface. *J. Chem. Soc., Faraday Trans.* **1995**, *91*, 1281–1296.
- (25) Buck, M.; Himmelhaus, M. Vibrational Spectroscopy of Interfaces by Infrared–Visible Sum Frequency Generation. *J. Vac. Sci. Technol., A* **2001**, *19*, 2717–2736.
- (26) Wang, H. F.; Gan, W.; Lu, R.; Rao, Y.; Wu, B. H. Quantitative Spectral and Orientational Analysis in Surface Sum Frequency Generation Vibrational Spectroscopy (SFG-VS). *Int. Rev. Phys. Chem.* **2005**, *24*, 191–256.
- (27) Zhang, H. P.; Romero, C.; Baldelli, S. Preparation of Alkanethiol Monolayers on Mild Steel Surfaces Studied with Sum Frequency Generation and Electrochemistry. *J. Phys. Chem. B* **2005**, *109*, 15520–15530.
- (28) Santos, G.; Baldelli, S. Scale Dependence of the Orientation and Conformation Distribution Analysis of a Molecular Monolayer Using Sum Frequency Generation Imaging Microscopy. *J. Phys. Chem. C* **2012**, *116*, 25874–25887.
- (29) Cimatu, K.; Baldelli, S. Spatially Resolved Surface Analysis of an Octadecanethiol Self-Assembled Monolayer on Mild Steel Using Sum Frequency Generation Imaging Microscopy. *J. Phys. Chem. C* **2007**, *111*, 7137–7143.
- (30) Park, J. S.; Vo, A. N.; Barriet, D.; Shon, Y. S.; Lee, T. R. Systematic Control of the Packing Density of Self-Assembled Monolayers Using Bidentate and Tridentate Chelating Alkanethiols. *Langmuir* **2005**, *21*, 2902–2911.
- (31) Cimatu, K. Sum Frequency Generation Imaging Microscopy. Ph.D. Thesis, University of Houston, 2008.
- (32) Bain, C. D.; Davies, P. B.; Ong, T. H.; Ward, R. N.; Brown, M. A. Quantitative-Analysis of Monolayer Composition by Sum-Frequency Vibrational Spectroscopy. *Langmuir* **1991**, *7*, 1563–1566.
- (33) Ong, T. H.; Davies, P. B.; Bain, C. D. Sum-Frequency Spectroscopy of Monolayers of Alkoxy-Terminated Alkanethiols in Contact with Liquids. *Langmuir* **1993**, *9*, 1836–1845.
- (34) Nishi, N.; Hobara, D.; Yamamoto, M.; Kakiuchi, T. Chain-Length-Dependent Change in the Structure of Self-Assembled Monolayers of *n*-Alkanethiols on Au(111) Probed by Broad-Bandwidth Sum Frequency Generation Spectroscopy. *J. Chem. Phys.* **2003**, *118*, 1904–1911.
- (35) Hautman, J.; Klein, M. L. Simulation of a Monolayer of Alkyl Thiol Chains. *J. Chem. Phys.* **1989**, *91*, 4994.
- (36) Hirose, C.; Akamatsu, N.; Domen, K. Formulas for the Analysis of Surface Sum-Frequency Generation Spectrum by CH Stretching

Modes of Methyl and Methylene Groups. *J. Chem. Phys.* **1992**, *96*, 997–1004.

(37) Hirose, C.; Yamamoto, H.; Akamatsu, N.; Domen, K. Orientation Analysis by Simulation of Vibrational Sum Frequency Generation Spectrum: CH Stretching Bands of the Methyl Group. *J. Phys. Chem.* **1993**, *97*, 10064–10069.

(38) Simpson, G. J.; Rowlen, K. L. Orientation-Insensitive Methodology for Second Harmonic Generation. 2. Application to Adsorption Isotherm and Kinetics Measurements. *Anal. Chem.* **2000**, *72*, 3407–3411.

(39) Jerkiewicz, G.; Vatankhah, G.; Lessard, J.; Soriaga, M. P.; Park, Y.-S. Surface-Oxide Growth at Platinum Electrodes in Aqueous H_2SO_4 . *Electrochim. Acta* **2004**, *49*, 1451–1459.

(40) Wei, X.; Hong, S.-C.; Zhuang, X.; Goto, T.; Shen, Y. Nonlinear Optical Studies of Liquid Crystal Alignment on a Rubbed Polyvinyl Alcohol Surface. *Phys. Rev. E* **2000**, *62*, 5160–5172.

(41) Huang, J. Y.; Shen, Y. R. Sum-Frequency Generation as a Surface Probe. In *Laser Spectroscopy and Photochemistry on Metal Surfaces*; Dai, H.-L., Ho, W., Eds.; World Scientific: Singapore, 1995; Vol. 5.

(42) Baldelli, S.; Bao, J.; Wu, W.; Pei, S.-s. Sum Frequency Generation Study on the Orientation of Room-Temperature Ionic Liquid at the Graphene–Ionic Liquid Interface. *Chem. Phys. Lett.* **2011**, *516*, 171–173.

(43) Simpson, G. J.; Westerbuhr, S. G.; Rowlen, K. L. Molecular Orientation and Angular Distribution Probed by Angle-Resolved Absorbance and Second Harmonic Generation. *Anal. Chem.* **2000**, *72*, 887–898.

(44) Wei, X.; Zhuang, X.; Hong, S.-C.; Goto, T.; Shen, Y. Sum-Frequency Vibrational Spectroscopic Study of a Rubbed Polymer Surface. *Phys. Rev. Lett.* **1999**, *82*, 4256–4259.

(45) Simpson, G. J.; Rowlen, K. L. Quantification of “Local” Surface Orientation: Theory and Experiment. *J. Phys. Chem. B* **1999**, *103*, 1525–1531.

(46) Hunt, J. H.; Guyot-Sionnest, P.; Shen, Y. R. Observation of C–H Stretch Vibrations of Monolayers of Molecules Optical Sum-Frequency Generation. *Chem. Phys. Lett.* **1987**, *133*, 189–192.

(47) Porter, M. D.; Bright, T. B.; Allara, D. L.; Chidsey, C. E. D. Spontaneously Organized Molecular Assemblies. 4. Structural Characterization of *n*-Alkyl Thiol Monolayers on Gold by Optical Ellipsometry, Infrared Spectroscopy, and Electrochemistry. *J. Am. Chem. Soc.* **1987**, *109*, 3559–3568.

(48) Laredo, T.; Leitch, J.; Chen, M.; Burgess, I. J.; Dutcher, J. R.; Lipkowski, J. Measurement of the Charge Number Per Adsorbed Molecule and Packing Densities of Self-Assembled Long-Chain Monolayers of Thiols. *Langmuir* **2007**, *23*, 6205–6211.

(49) Chechik, V.; Schönher, H.; Vancso, G. J.; Stirling, C. J. M. Self-Assembled Monolayers of Branched Thiols and Disulfides on Gold: Surface Coverage, Order and Chain Orientation. *Langmuir* **1998**, *14*, 3003–3010.

(50) Strong, L.; Whitesides, G. M. Structures of Self-Assembled Monolayer Films of Organosulfur Compounds Adsorbed on Gold Single Crystals: Electron Diffraction Studies. *Langmuir* **1988**, *4*, 546–558.

(51) Shon, Y.-S.; Colorado, R.; Williams, C. T.; Bain, C. D.; Lee, T. R. Low-Density Self-Assembled Monolayers on Gold Derived from Chelating 2-Monoalkylpropane-1,3-Dithiols. *Langmuir* **2000**, *16*, 541–548.